IJMMM International Journal of Minerals, Metallurgy and Materials 矿物冶金与材料学报（英文版）

Effects of Zr content on electrochemical performance of Ti/Sn–Ru–Co–ZrO_x electrodes

Linhui Chang, Sheng Chen, Xionghui Xie, Buming Chen, Haihong Qiao, Hui Huang, Zhongcheng Guo, and Ruidong Xu

Cite this article as:
Linhui Chang, Sheng Chen, Xionghui Xie, Buming Chen, Haihong Qiao, Hui Huang, Zhongcheng Guo, and Ruidong Xu, Effects of Zr content on electrochemical performance of Ti/Sn–Ru–Co–ZrO_x electrodes, *Int. J. Miner. Metall. Mater.*, 29(2022), No. 12, pp. 2181-2188. https://doi.org/10.1007/s12613-021-2326-y

View the article online at SpringerLink or IJMMM Webpage.

International Journal of Minerals, Metallurgy and Materials
Volume 29, Number 12, December 2022, Page 2181
https://doi.org/10.1007/s12613-021-2326-y

Effects of Zr content on electrochemical performance of Ti/Sn–Ru–Co–ZrO_x electrodes

Linhui Chang[1,2], *Sheng Chen*[1,2], *Xionghui Xie*[1], *Buming Chen*[1,2,3]✉, *Haihong Qiao*[4], *Hui Huang*[1,2,3], *Zhongcheng Guo*[1,2,3], *and Ruidong Xu*[1]

1) Faculty of Metallurgical and Energy Engineering, Kunming University of Science and Technology, Kunming 650093, China
2) Research Center of Metallurgical Electrode Materials Engineering Technology, Kunming 650106, China
3) Kunming Hendera Science and Technology Co., Ltd., Kunming 650106, China
4) North Night Vision Technology Research Institute Group Co., Ltd. Optical Company, Kunming 650093, China
(Received: 22 March 2021; revised: 2 July 2021; accepted: 5 July 2021)

Abstract: The low cell voltage during electrolytic Mn from the $MnCl_2$ system can effectively reduce the power consumption. In this work, the Ti/Sn−Ru−Co−Zr modified anodes were obtained by using thermal decomposition oxidation. The physical parameters of coatings were observed by SEM (scanning electron microscope). Based on the electrochemical performance and SEM/XRD (X-ray diffraction) of the coatings, the influence of Zr on electrode performance was studied and analyzed. When the mole ratio of Sn−Ru−Co−Zr is 6:1:0.8:0.3, the cracks on the surface of coatings were the smallest, and the compactness was the best due to the excellent filling effect of ZrO_2 nanoparticles. Moreover, the electrode prepared under this condition had the lowest mass transfer resistance and high chloride evolution activity in the 1mol% NH_4Cl and 1.5mol% HCl system. The service life of 3102 h was achieved according to the empirical formula of accelerated-life-test of the new type anode.

Keywords: Ti/Sn−Ru−Co−Zr anode; electrochemical; Mn electrowinning; manganese chloride system; service life

1. Introduction

In the recent industrial electrodeposition of Mn, the sulfate and chloride systems were commonly used. Oxygen evolution reaction (OER), and chlorine evolution reaction (CER) mainly occur at the anode in the sulfuric acid system and the chlorination system, respectively.

Pb-based alloy anodes [1] have long been used for electrolytic extraction of Mn in a sulfate system. The corrosion resistance of the Pb−1wt%Ag anodes with railing structure [2] was 4.3 times that of ordinary boards in an acid solution. The excellent corrosion resistance benefits from the formation of a PbO_2 protective film with good conductivity on the Pb surface in the acidic solution. Pb−Sn−1wt%Ag−Sb anodes [3] were beneficial to the precipitation of metallic Mn because of the low output of MnO_2. Compared with the Pb−Sn−1wt%Ag−Sb anodes, the new Pb−Ag−Ca alloy [4] greatly reduced the amount of Ag consumption and early corrosion, the current efficiency was increased by 3.3% also. Although the new Pb-based alloys were more environmentally friendly, especially in energy consumption, the powdery MnO_2 with high electrochemical activity is generated in the solution during electrolysis when using Pb-based alloys. MnO_2 products would be contaminated by dissolved Pb impurities, which was not conducive for a long-term application.

There were many shortcomings during producing Mn by electrolysis in the sulfate system ($MnSO_4$–$(NH_4)_2SO_4$–H_2O), such as low current efficiency, high energy consumption, and serious pollution [5]. However, in the chloride ($MnCl_2$–NH_4Cl–H_2O) electrolysis system, although there are Cl_2 releasing and the corrosion of the anode by the overflow Cl_2, the high electrolyte conductivity and high manganese deposition efficiency still kept. The above advantages and the low energy consumption had attracted the attention of many researchers [6]. Compared with the sulfate system, high purity Mn was obtained by the diaphragm electrolysis in the chloride system with low cell voltage and high current efficiency [7−8]. The strong adsorption of $MnCl^+$ on the cathode inhibited H_2 evolution in the chloride solution and was conducive to the rapid nucleation of metals and the deposition of fine crystals, mainly generating a large-scale γ-Mn crystal system [9]. The Ti/PbO_2 electrodes [10] were successfully used instead of graphite anodes to prepare high-quality electrolytic Mn from the $MnCl_2$ system. This allows high Mn^{2+} concentration and high current density to be used, and the amount of Cl_2 escape is greatly reduced. The anodes usually working in a strong acidic and high current density environment [11] by

✉ Corresponding author: Buming Chen E-mail: bumchen@kust.edu.cn

using IrO_2, RuO_2 [12] to maintain high activity. The stability of the electrodes was improved by other inert elements, such as TiO_2, Ta_2O_5 [13]. It was found that Ti/IrO_2 (70mol%)–Ta_2O_5 (30mol%) coated anode has high electrocatalytic activity and stability in an acidic environment. Meanwhile, to improve the stability of the Ti-based coating, other metal oxides were doped in the intermediate layer, such as Co/Sb doped Ti/SnO_2 electrode [14]. This oxide intermediate layer prevented the oxygen precipitated in the reaction from diffusing into the Ti substrate and the generation of non-conductive TiO_2 or other Ti oxides, so the service life of the electrode was increased [15–18]. Thus, the replacement of traditional Pb–Ag anodes by Ti-based rare metal oxide coating anodes is very valuable.

Based on the preparation of the prescriptive Ti/Sn–Ru–Co oxide electrodes, a new type of Ti/Sn–Ru–Co–Zr oxide electrode was prepared by multiple thermal decomposition oxidation with different content of Zr. The new Ti/Sn–Ru–Co–Zr anodes were investigated, and their stability of surface morphology and phase performance were compared with no Zr added electrodes. In addition, the performance of the electrode was studied by the electrochemical station.

2. Experimental

2.1. Sample preparation

2.1.1. Pretreatment of Ti matrix

This process was three steps in the pre-treated titanium substrate [19]. First, the Ti sheets (1 cm × 3 cm × 0.1 cm) were dipped into 10wt% NaOH solution at 70°C for 30 min and then rinsed with deionized water to remove grease. Secondly, the Ti sheets were etched in mixed acid solution (HF : HNO_3 : H_2O = 1:4:5 in volume ratio) for 3 min to remove the oxide layer, and repeated the rinsing work in the previous step. Next, etching the Ti sheets in 20wt% HCl solution at 90°C for 2 h to shape into a rough surface. Particularly, the pretreated Ti substrates were stored in ethanol solution at 25°C before use.

2.1.2. Preparation of oxide coating

A mixture of $SnCl_4{\cdot}5H_2O$, $RuCl_3{\cdot}3H_2O$, $CoCl_2{\cdot}6H_2O$, and Zr $(NO_3)_2$ was dissolved in 20wt% HCl and n-butanol at molar ratio 6:1:0.8: x (Sn = 0.006 mol; x = 0, 0.1, 0.3, 0.5, 0.7) was used as the precursor. The mixtures were completely and uniformly dissolved under an ultrasonic wave. Then, the precursor solution is painted to the pre-treated Ti substrates by using a brush. The Ti sheets were heated at a stable temperature of 500°C for 10 min after drying at 100°C. The sheets were brushed again after air-cooled to room temperature. The whole procedure was repeated 13 times and the last was heated for 1 h. After the above processes, 12–14 g/m^2 oxide was loaded on the surface of the Ti sheets.

2.2. Characterization and electrochemical analysis

The surface morphology of the coatings and crystal structure were examined by scanning electron microscopy (SEM, SU8010, HITACHI, Japan). The phase composition of the coating was surveyed by XRD (X-ray diffraction) (RIGAKU D / MAX 2550, Japan) with Cu K_α radiation. The electrochemical tests were performed on an electrochemical workstation (RST-5200, China) with three-electrode systems. In an electrolyte solution of 1.5mol% HCl and 1mol% NH_4Cl, the temperature was kept at 40°C. The working area is a single-sided insulated 1.0 cm^2 electrode. The reference electrode was the saturated calomel electrode (SCE), and a Pt sheet of 6.0 cm^2 was used as the auxiliary electrode. The corresponding potential range for linear sweep voltammetry (LSV) testing was 0.4–1.4 V with a scanning rate of 10 mV/s. The cyclic voltammetry (CV) testing was 0.5–0.9 V with a scanning rate of 1 mV/s, and EIS (electrochemical impedance spectroscopy) examination was conducted with an AC (alternating current) amplitude at 5 mV in the frequency range of 10^5 to 10^{-2} Hz. The additional anode potential was 1.2 V. The impedance data were converted into Nyquist data and fitted with expedient analog circuits. As shown in Fig. 1, the model was connected to the electrochemical workstation.

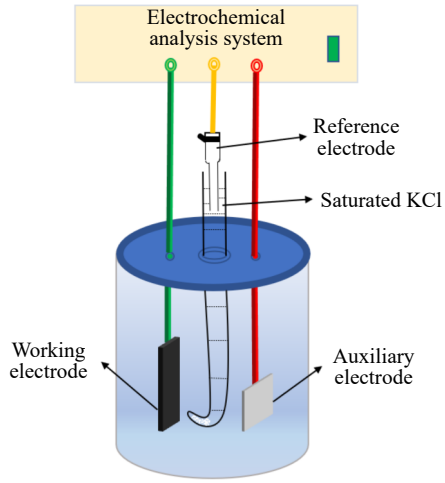

Fig. 1. Schematic of electrochemical measurements.

To shorten the experimental period, the accelerated life test of this anode coatings was evaluated using a solution containing 10wt%H_2SO_4, at 40°C with 1070-Al as the cathode. The distance between the electrodes was 2 cm, and the current density was 2 A/cm^2. The empirical relationship between accelerated life t_1 and actual service life t_2 was as follows [19].

$$t_2 = \left(\frac{J_2}{J_1}\right)^n t_1 \tag{1}$$

where n is a constant, usually taken as 2, J_1 means the actual current density, and J_2 denotes the accelerated current density.

3. Results and discussion

3.1. XRD analysis of oxide coating

The effect of coating phase with different Zr content measured by XRD is displayed in Fig. 2. The coating is mainly composed of oxides, including the crystalline phases of SnO_2, RuO_2, and ZrO_2. The diffraction peaks of ZrO_2 and RuO_2 were overlapped together, indicating that solid solution probably formed between them. Through card analysis

(JCPDS: RuO_2-No.40-1290; SnO_2-No.41-1445; ZrO_2-No.37-1484; Ti-No.44-1294), it was observed that the crystal spacing *d* of diffraction peaks was close to that of RuO_2, which is attributed to the main ruthenium-based solid solution. Furthermore, with the increase of Zr content according to XRD, the oxidation peak of the electrode coating first weakened and then enhanced. When the molar ratio of Sn : Ru : Co : Zr is 6:1:0.8:0.3, each diffraction peak was the weakest. In addition, with the increase of Zr content, the RuO_2 of the (211) crystal plane increases significantly than that of SnO_2. The solid solution of RuO_2 and ZrO_2 was turned into the crystal by strengthening and help form more stable structure. Otherwise, the intensity of Ti diffraction peak on the (101) crystal plane decreased with the increase of Zr content. However, when Sn : Ru : Co : Zr is 6:1:0.8:0.3, only trace amounts of titanium were found in the coating, indicating that the grains were refined and the Ti matrix was protected from corrosion by the addition of Zr.

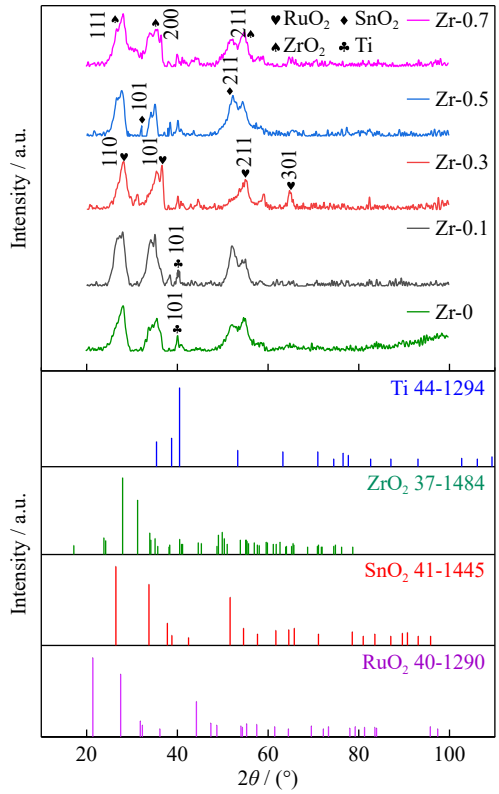

Fig. 2. XRD patterns of electrodes prepared with different Zr contents.

3.2. SEM analysis of oxide coating

The SEM images of the different Zr content electrodes were given in Fig. 3. The surface morphology of the electrodes changed with the content of Zr. The electrochemical activity for the electrodes was related to the roughness of the electrode's surface certainly [20]. It can be obtained from Fig. 3 that with the increase of Zr content, the surface cracks first decreased and then increased. When the molar ratio of Sn : Ru : Co : Zr is 6:1:0.8:0.3, the surface morphology cracks were the least. The substrate was well protected from the corrosion of the solution during electrolysis due to the dense surface. As shown in Fig. 3(c), an amount of rough morphology appeared upon the electrode surface, and the rough morphology was able to protect the matrix from solution erosion [20]. The X-ray dot-mapping test was performed on the Zr-0.3 added electrode, focusing on the distribution of Zr element and the protective effect on the Ti matrix. The results showed that the distribution of Zr element on the coating particles was uniform, the coating had a good protective effect on the titanium substrate, and only a small amount of Ti element was exposed.

3.3. Chlorine evolution activity of oxide coated electrode

The anodic polarization curve testing results were shown in Fig. 4. At 500 A/m^2, the chlorine evolution potential of

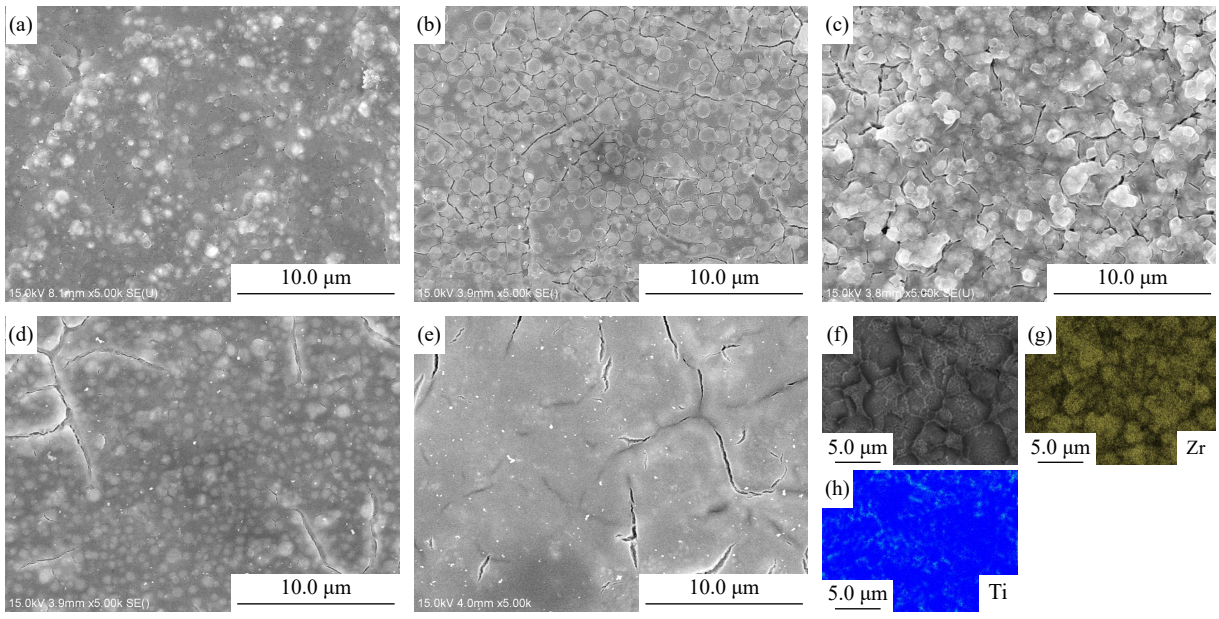

Fig. 3. SEM images of the electrodes prepared with different Zr contents: (a) Zr-0; (b) Zr-0.1; (c) Zr-0.3; (d) Zr-0.5; (e) Zr-0.7. (f–h) Mapping of Zr-0.3 anode.

Ti/Sn–Ru–Co–Zr oxide coated anode with different Zr content was 1.238 V (Zr-0), 1.221 V (Zr-0.1), 1.210 V (Zr-0.3), 1.259 V (Zr-0.5), and 1.311 V (Zr-0.7), respectively. By comparing the above data, it is easy to calculate the potential difference of chlorine evolution, which was 101 mV. These potentials related to the level of chlorine evolution activity indicating that the Zr-0.3 electrode had the strongest chlorine evolution activity.

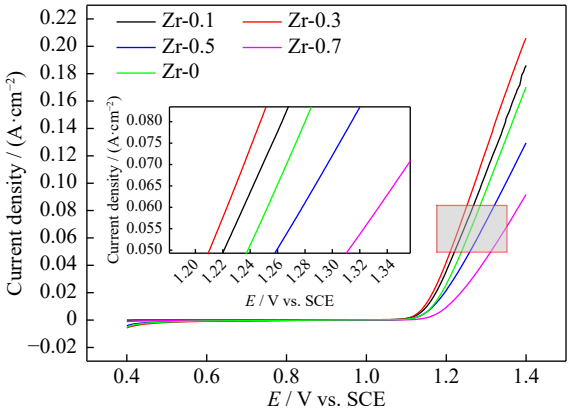

Fig. 4. Anodic polarization curves of electrodes prepared with different Zr contents and partial enlarged view around 500 A/m^2.

The value of the polarization curve and chlorine release activity can be determined by comparing the overpotential of evolution [20]. The potential value was corrected by using Eq. (2) to describe the overpotential of chlorine evolution reaction (CER, η) of electrode material [21]:

$$\eta = E + 0.241 - 1.260 - iR_s \tag{2}$$

where E denotes the CER measured by the anode polarization curve in the experiment [22], and 1.260 V was the standard potential in the measurement system (1.5mol% HCl and 1mol% NH_4Cl, 40°C). i is the current density measured at the relative potential. R_s is the electrolyte resistance between the reference electrode and the working electrode. The equilibrium potential of chlorine release was calculated by the Nernst equation. The potential of SCE was 0.241 V compared with the standard hydrogen electrode.

The chlorine evolution overpotential η has a semi-logarithmic relationship with the current density J, as shown in Eq. (3):

$$\eta = a + b\lg J \tag{3}$$

where a is a constant for the anodic process, V; b is the Tafel slope, V·dec^{-1}.

$$a = -2.3(RT/\beta nF)\lg J_0 \tag{4}$$

$$b = 2.3RT/\beta nF \tag{5}$$

where R is the constant of gas; T is the temperature; β is the transfer coefficient, which represents the influence of the electrode potential on the anodic reaction; n represents the number of transferred electron; F is the Faraday's constant; J_0 is the exchange current density.

According to Fig. 5 and the data in Table 1, under the following conditions about 500 and 1000 A/m^2, when the molar ratio of Sn : Zr is 6:0.3, the chlorine evolution overpotential was the lowest, about 0.143 V and 0.218 V, respectively. The small value indicated that the evolution of chlorine was easier. The value of "a" was positively correlated with the size of cell voltage. The depolarization phenomenon was related to a large amount of oxide with electrocatalytic activity in the coating, and the nanoparticles formed by adding an appropriate amount of Zr in the coating were very helpful, so the Zr-0.3 electrode had the lowest voltage. Scilicet, the above-mentioned oxide electrode coating had high catalytic activity.

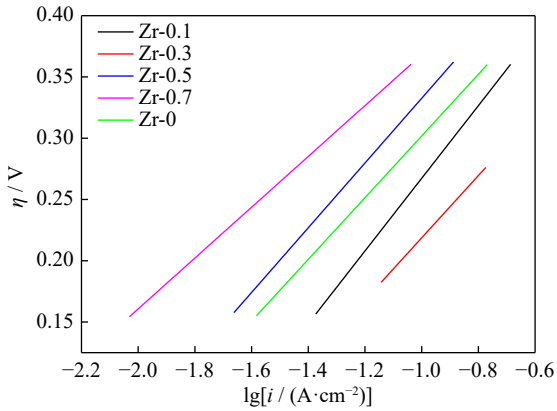

Fig. 5. Fitted Tafel lines of coatings prepared with different Zr contents.

Table 1. Overpotential and fitted value for chlorine evolution with different Zr contents

Name	η / V		a / V	b / (V·dec^{-1})
	500 A·m^{-2}	1000 A·m^{-2}		
Zr-0.1	0.178	0.267	0.563	0.296
Zr-0.3	0.143	0.218	0.473	0.254
Zr-0.5	0.253	0.333	0.597	0.264
Zr-0.7	0.306	0.368	0.575	0.207
Zr-0	0.226	0.302	0.554	0.252

Fig. 6 showed the EIS curves of the different samples. A half-circle could be observed of all curves present with basically the same shape. The capacitive properties of the electrode impedance radius first decrease and then increase.

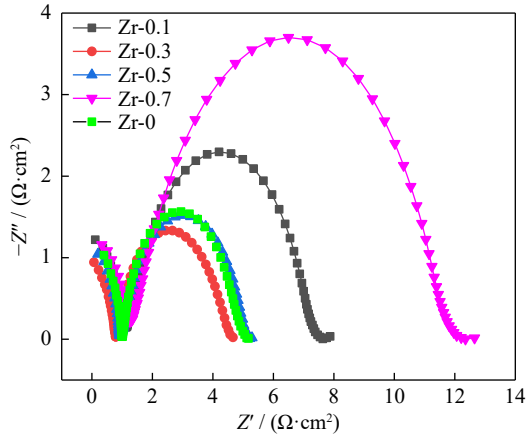

Fig. 6. EIS curves of film-forming anode sample with different Zr contents.

Moreover, the capacitive reactance arc radius prepared under the molar ratio of Sn : Zr = 6:0.3 was the smallest, which indicated that the resistance to electron transfer was the lowest and the number of electron transfer per unit time was the most. ZrO_2 particles accumulated on an anode surface influence the electric double layer structure and decrease the effective area of other metal oxides on the dimentionally stable anode surface [21]. The accumulation of ZrO_2 particles results in the increment of impedance value from the RuO_2 system with ZrO_2 particles.

In Fig. 7, (R_S ($Q_{dl}R_{ct}$) (Q_fR_f)) was regarded as the equivalent model used to fit the pseudo data [22]. Among them, R_S means solution resistance; Q_f signifies internal crack of coating and grain boundary pore structure; R_f indicates the resistance of the electrode itself; Q_{dl} is often used to characterize the number of active points, and the higher the value of Q_{dl}, the more active points are loaded on the surface; R_{ct} represents the activity of chlorine released from the electrode, and the lower the value of R_{ct}, the better the electrocatalytic activity of chlorine evolution of the electrode.

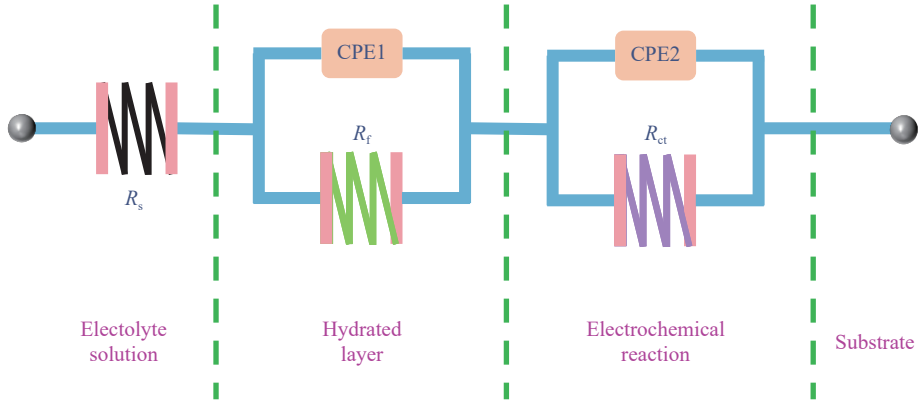

Fig. 7. Impedance fitting model.

According to Fig. 6 and Table 2, with the increase of Zr content, R_{ct} first decreases and then increases. The charge mass transfer resistance of the electrode prepared under the molar ratio of Sn : Zr = 6:0.3 was the smallest, suggested that the electrode prepared under this condition was the most prone to chlorine evolution reaction. Otherwise, with the increase of Zr content, Q_{dl} first increases and then decreases. The Q_{dl} under the condition of Sn : Zr = 6:0.3 was the largest, indicated that the coating surface of the electrodes prepared under this condition contains the most active sites.

Table 2. Fitting parameter of EIS curves

Sample	R_s / (Ω·cm^2)	Q_f / (μF·cm^{-2})	n	R_f / (Ω·cm^2)	Q_{dl} / (μF·cm^{-2})	Calculated roughness factor	R_{ct} / (Ω·cm^2)
Zr-0.1	1.0×10^{-5}	2.01	1	1.270	8600	430	6.062
Zr-0.3	2.6×10^{-7}	2.70	1	0.892	68900	3445	3.501
Zr-0.5	2.7×10^{-7}	2.19	1	1.040	39700	1985	4.014
Zr-0.7	1.1×10^{-6}	1.83	1	1.371	4400	220	10.490
Zr-0	9.7×10^{-7}	2.66	1	0.759	32400	1620	4.678

The cyclic voltammetry curve was integrated to obtain the q^*, which reflects the electrochemical activity of the electrode, and was related to the practical working area and the number of active points. A large value of q^* illustrates great electrode activity. Using this method by some previous report [23–24] to calculate the q^* value to estimate the electrode activity, and the equation is:

$$(q^*)^{-1} = (q_T)^{-1} + kv^{1/2} \quad (6)$$

herein, q_T means the real charge on the electrode surface, $kv^{1/2}$ delegates the reciprocal of the square of the charge and the scanning rate [25].

The CV curves of Ti/Sn–Ru–Co–ZrO_x samples in the whole potential range of 0.5–0.9 V was shown in Fig. 8. q^* was measured in acidic NH_4Cl solution to define the electrochemically active area of the Ti/Sn–Ru–Co–ZrO_x electrodes. Thus, the value of q^* was defined as the electrochemically active surface area of Ti/Sn–Ru–Co–ZrO_x in chlorate electrolyte. Obviously, with the increase of Zr content, the active area of the electrode first increased and then decreased, and the area enclosed by the CV of the Ti/Sn–Ru–Co–ZrO_x electrodes prepared at the molar ratio of Sn : Zr = 6:0.3 was the largest. The second was the Ti/Sn–Ru–Co–ZrO_x electrode prepared under the condition of Sn : Zr = 6:0.5. Too much Zr leads to excessive inert oxides on the surface of the electrode, which reduces the electrocatalytic activity of the electrode. Therefore, the active area of the Zr-0.7 added electrode was the smallest. It was also confirmed that the electrode with low chlorine emission potential had more active sites and higher chlorine emission activity. Owing to smaller grain size was favored to the formation of the large active surface area [26]. The active surface areas of Zr-0.3 electrodes were optimal. As known that larger specific area was beneficial to improve the catalytic properties, so the Zr-0.3 electrodes owned high-

er electrocatalysis activity than others. When Zr was added into the precursor solution, ZrO_2 nanoparticles were formed during thermal oxidation and effectively embedded in the matrix. The pores were filled by a handful of ZrO_2 nanoparticles to reduce the grain size of the others dioxide matrix [27–28], as shown in Fig. 3(c). The dense membrane prevented the electrolyte from penetrating through cracks or pores. Moreover, there was no high pressure inside the coating since the generation of internal Cl_2 was reduced [29]. Hence, the probability of perforation of the coating was minimal. The above reasons were combined to make the Zr-0.3 electrode has an excellent electrochemical performance.

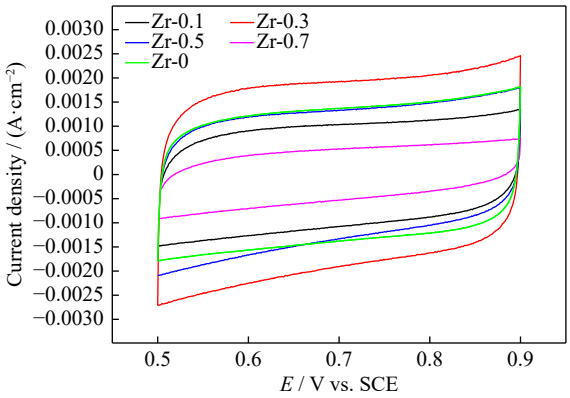

Fig. 8. CV curves of coatings prepared with different Zr contents.

In addition, the approximate actual life was estimated by an accelerated life test. The current used in accelerated life tests is much higher than that in actual use. According to the above electrochemical test, the best performance was obtained by the molar ratio of Sn : Zr = 6:0.3, so the accelerated life test was taken to compare with that without Zr. The accelerated life test results of the electrodes were shown in Fig. 9, and the failure judged according to the voltage reachs 10 V. Absolutely the voltage of all samples quickly reached a stable state in a short time (500 h) at the beginning of the test. Hereafter, the electrode potential remained unchanged. The voltage of the coating with Zr was slightly higher than that of the coating without Zr, which was consistent with the R_f data that was fitted in Table 2. At last, the potential rose sharply and the electrode failed. The corresponding working times were 3102 h (Zr-0.3) and 2773 h (Zr-0), respectively. The electrode service life can be extended about 11.86% by adding Zr-0.3.

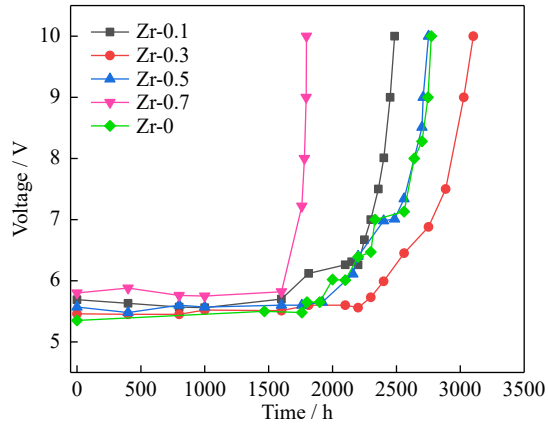

Fig. 9. Accelerated life test result of Zr added electrode.

Attributed to the appropriate ZrO_2 weight percentage in electrodes, the ZrO_2 nanoparticles acted as an inert physical barrier that initiates corrosion of the substrate [30], and prevented the electrolyte from reaching the Ti surface effectively [31]. As shown in Fig. 10, the SEM images of two electrodes after the corrosion experiment were given, and the protection mechanism of nano-ZrO_2 on the coating was proposed. In Fig. 10(a), it can be seen that there was a deep color different from that in Fig. 10(b). The corrosion pits on the surface were deeper here because there was no protection from Zr. The protection provided was positively related to the amount of ZrO_2 nanoparticles when the Zr content was low, and these appropriate amount of ZrO_2 particles (Sn : Zr = 6:0.3 in this work) would fill the gaps between the oxide coatings and link the bulk coatings to each other to better protect the Ti substrate. Due to the large specific surface area on the surface of the electrode, under the same apparent current density, its actual current density is actually low, so its sur-

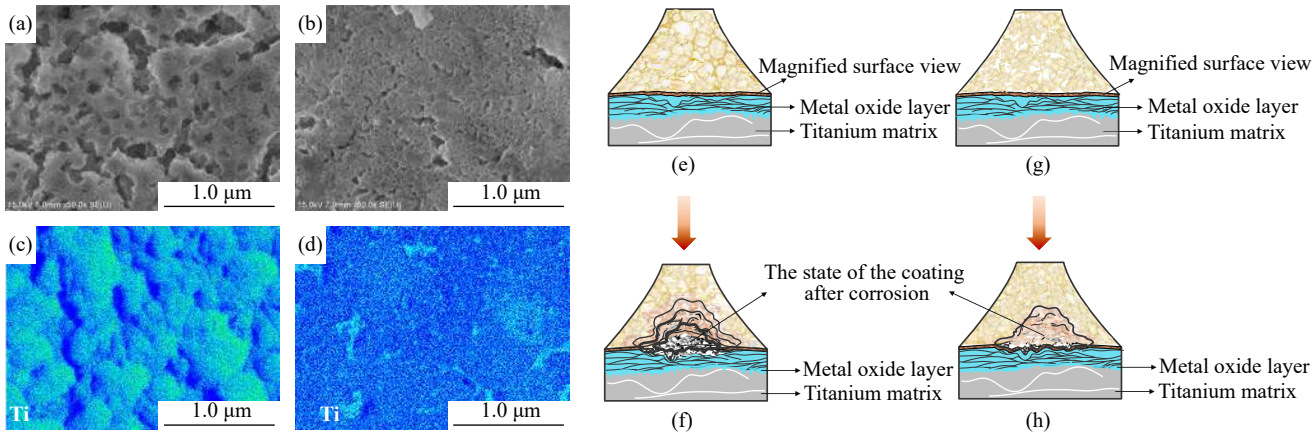

Fig. 10. SEM images and mapping analysis of the anode samples after corrosion experiments: (a, c) Zr-0; (b, d) Zr-0.3. Protection mechanism of the anode samples in corrosion experiments: (e, f) Zr-0 anode before and after corrosion; (g, h) Zr-0.3 anode before and after corrosion.

face corrosion is relatively low. Otherwise, the Cl_2 evolution reaction mainly occurs on the surface of the electrode, and the electrode with a larger specific surface area has better electrochemical activity. However, the good protective effect on the titanium matrix is the key to increasing the use time instead of the surface. From the comprehensive performance test results and accelerated life test results, a certain amount of Zr addition is beneficial. Furthermore, after the addition of Zr exceeded a certain amount (Sn : Zr = 6:0.5 in this work), the coating bonded with the substrate loosely, thereby affecting its performance. Therefore, the service life of Zr-0.3 electrodes improved greatly.

4. Conclusions

To obtain a more corrosion-resistant and economical electrolytic anode, based on the traditional Ti/Sn–Ru–CoO_x coating, Zr was added to modify the electrode. A series of Ti/Sn–Ru–Co–ZrO_x electrodes with different Zr contents were prepared by the thermal decomposition method.

(1) With the increase of Zr content, the densification of electrode surface increased first and then decreased. The surface of the Zr-0.3 electrode was the most compact.

(2) Under the condition of Sn : Ru : Co : Zr = 6:1:0.8:0.3 (in molar ratio), the electrode had the largest active area and the best catalytic performance, as confirmed by the electrochemical testing results.

(3) The Zr modified electrode remained stable for up to 3102 h (empirical formula estimation) in a solution with 10wt% H_2SO_4 at 40°C under 2 A/cm^2. This anode was more stable than the no Zr added anode, the serves life expectancy was increased about 11.86%.

Acknowledgements

This work was financially supported by the National Natural Science Foundation of China (Nos. 51564029, 51504111, 52064028, and 22002054), the China Postdoctoral Science Foundation (No. 2018M633418), the Technology Innovation Talents Project of Yunnan Province (No. 2019HB111), and Analysis and Testing Foundation of Kunming University of Science and Technology (Nos. 2019 M20182202013, 2020M20192202035, and 2020M2019 2202099).

Conflict of Interest

The authors declare no potential conflict of interest.

References

[1] J.M. Lu, D. Dreisinger, and T. Glück, Manganese electrodeposition—A literature review, *Hydrometallurgy*, 141(2014), p. 105.

[2] S.K. Padhy, P. Patnaik, B.C. Tripathy, M.K. Ghosh, and I.N. Bhattacharya, Electrodeposition of manganese metal from sulphate solutions in the presence of sodium octyl sulphate, *Hydrometallurgy*, 165(2016), p. 73.

[3] G. Tsurtsumia, D. Shengelia, N. Koiava, *et al*., Novel hydro-electrometallurgical technology for simultaneous production of manganese metal, electrolytic manganese dioxide, and manganese sulfate monohydrate, *Hydrometallurgy*, 186(2019), p. 260.

[4] E. Rocca, G. Bourguignon, and J. Steinmetz, Corrosion management of PbCaSn alloys in lead-acid batteries: Effect of composition, metallographic state and voltage conditions, *J. Power Sources*, 161(2006), No. 1, p. 666.

[5] E. Rudnik, Effect of gluconate ions on electroreduction phenomena during manganese deposition on glassy carbon in acidic chloride and sulfate solutions, *J. Electroanal. Chem.*, 741(2015), p. 20.

[6] J.E. Lewis, P.H. Scaife, and D.A.J. Swinkels, Electrolytic manganese metal from chloride electrolytes. I. Study of deposition conditions, *J. Appl. Electrochem.*, 6(1976), No. 3, p. 199.

[7] X.Z. Cao, D.B. Dreisinger, J.M. Lu, and F. Belanger, Electrorefining of high purity manganese, *Hydrometallurgy*, 171(2017), p. 412.

[8] A. Sulcius, E. Griskonis, K. Kantminiene, and N. Zmuidzinaviciene, Influence of different electrolysis parameters on electrodeposition of γ- and α-Mn from pure electrolytes—A review with special reference to Russian language literature, *Hydrometallurgy*, 137(2013), p. 33.

[9] P. Wei, O.E. Hileman Jr, M.R. Bateni, X.H. Deng, and A. Petric, Manganese deposition without additives, *Surf. Coat. Technol.*, 201(2007), No. 18, p. 7739.

[10] Y.X. Zheng, Preparation of electrolytic manganese metal from $MnCl_2$ system with graphite substract lead dioxide anode, *China Manganese Ind.*, 16(1998), No. 3, p. 30.

[11] W.C. Yang, W.J. Peng, X.H. Li, *et al*., Preparation of titanium-substrate modified Ti/SnO_2/MnO_2 anode plate for electrolytic manganese metal and its performance study, *Min. Metall. Eng.*, 34(2014), No. 3, p. 90.

[12] Y.Q. Wen, W. Shang, B.H. Xie, C.B. He, Y.Y. Wang, and D. Kong, Preparation and properties of composite coating modified titanium anode for electrolytic manganese dioxide, *China Surf. Eng.*, 30(2017), No. 2, p. 85.

[13] J.M. Hu, H.M. Meng, J.Q. Zhang, and C.N. Cao, Degradation mechanism of long service life Ti/IrO_2–Ta_2O_5 oxide anodes in sulphuric acid, *Corros. Sci.*, 44(2002), No. 8, p. 1655.

[14] E. Horváth, J. Kristóf, L. Vázquez-Gómez, Á. Rédey, and V. Vágvölgyi, Investigationof RuO_2–IrO_2–SnO_2 thin film evolution, *J. Therm. Anal. Calorim.*, 86(2006), No. 1, p. 141.

[15] Z.X. Zhang and D. Huang, *Coated Titanium Electrode,* Metallurgical Industry Press, Beijing, 2014, p. 62.

[16] Y.Y. Chen, T. Zhang, X. Wang, Y.Q. Shao, and D. Tang, Phase structure and microstructure of a nanoscale TiO_2–RuO_2–IrO_2–Ta_2O_5 anode coating on titanium, *J. Am. Ceram. Soc.*, 91(2008), No. 12, p. 4154.

[17] W. Zhang, E. Ghali, and G. Houlachi, Review of oxide coated catalytic titanium anodes performance for metal electrowinning, *Hydrometallurgy*, 169(2017), p. 456.

[18] H. You, Y.H. Cui, Y.J. Feng, J.F. Liu, and W.M. Cai, Preparation and performance of SnO_2 electrocatalytic electrode with titanium-based Co interlayer, *Mater. Sci. Technol.*, 12(2004), No. 3, p. 230.

[19] L.H. Chang, B.M. Chen, H.H. Qiao, *et al*., Study of the effects of pretreatment processing on the properties of metal oxide coatings on Ti-based sheet, *J. Electrochem. Soc.*, 168(2021), No. 3, art. No. 033501.

[20] D.P. Wang, G. Chen, A.D. Wang, *et al*., Corrosion behavior of single- and poly-crystalline dual-phase TiAl–Ti3Al alloy in NaCl solution, *Int. J. Miner. Metall. Mater*, 2022. DOI: 10.1007/s12613-022-2513-5

[21] R.D. Xu, L.P. Huang, J.F. Zhou, P. Zhan, Y.Y. Guan, and Y. Kong, Effects of tungsten carbide on electrochemical proper-

ties and microstructural features of Al/Pb–PANI–WC composite inert anodes used in zinc electrowinning, *Hydrometallurgy*, 125-126(2012), p. 8.

[22] J.H. Huang, M.J. Hou, J.Y. Wang, *et al*., RuO_2 nanoparticles decorate belt-like anatase TiO_2 for highly efficient chlorine evolution, *Electrochimica Acta*, 339(2020), art. No. 135878.

[23] B.M. Chen, S.C. Wang, J.H. Liu, *et al*., Corrosion resistance mechanism of a novel porous Ti/Sn–Sb–RuO_x/β-PbO_2 anode for zinc electrowinning, *Corros. Sci.*, 144(2018), p. 136.

[24] S. Trasatti, Structure of the metal/electrolyte solution interface: New data for theory, *Electrochimica Acta*, 36(1991), No. 11-12, p. 1659.

[25] H. Vogt, Note on a method to interrelate inner and outer electrode areas, *Electrochimica Acta*, 39(1994), No. 13, p. 1981.

[26] Y. Chen, L. Hong, H.M. Xue, *et al*., Preparation and characterization of TiO_2-NTs/SnO_2–Sb electrodes by electrodeposition, *J. Electroanal. Chem.*, 648(2010), No. 2, p. 119.

[27] Y.W. Yao, M.M. Zhao, C.M. Zhao, and H.J. Zhang, Preparation and properties of PbO_2–ZrO_2 nanocomposite electrodes by pulse electrodeposition, *Electrochimica Acta*, 117(2014), p. 453.

[28] Y.W. Yao, T. Zhou, C.M. Zhao, Q.M. Jing, and Y. Wang, Influence of ZrO_2 particles on fluorine-doped lead dioxide electrodeposition process from nitrate bath, *Electrochim. Acta*, 99(2013), p. 225.

[29] Y.H. Song, G. Wei, and R.C. Xiong, Structure and properties of PbO_2–CeO_2 anodes on stainless steel, *Electrochim. Acta*, 52(2007), No. 24, p. 7022.

[30] J.H. Liu, B.M. Chen, S. Chen, S.C. Wang, Z.C. Guo, Preparation and electrochemical performance of the stainless steel/α-PbO_2–ZrO_2/β-PbO_2–ZrO_2-CNT composite anode, *ECS J. Solid State Sci. Technol.*, 9(2020), No. 12, art. No. 121011.

[31] H. Mazhari Abbasi, K. Jafarzadeh, and S.M. Mirali, An investigation of the effect of RuO_2 on the deactivation and corrosion mechanism of a Ti/IrO_2+Ta_2O_5 coating in an OER application, *J. Electroanal. Chem.*, 777(2016), p. 67.